

A low-cost terrestrial stereo-pair photogrammetric monitoring system for highly hazardous areas

DE Guccione *The University of Newcastle, Australia*

A Giacomini *The University of Newcastle, Australia*

K Thoeni *The University of Newcastle, Australia*

F Bahootoroody *The University of Newcastle, Australia*

R Roncella *University of Parma, Italy*

Abstract

Spatial data are nowadays commonly used in engineering practice to support geohazard managements, identify and classify possible instabilities, and monitor their activity. Terrestrial laser scanners and ground-based radar systems, often implemented in mobile vehicles, are widely used within the mining sector to conduct periodic surveys of extended areas of hazardous access, and track deformations in almost real time. While such systems are very accurate and can operate in various weather conditions, their utilisation could incur substantial costs and require high technical expertise. Photogrammetry is considered as a viable and cost-effective alternative to traditional slope monitoring techniques. This paper presents recent improvements of a low-cost, autonomous terrestrial stereo-pair photogrammetric monitoring system specifically developed by the authors to monitor highly hazardous areas in surface mining environments and its application to the monitoring of a highwall face located in a mine site in New South Wales (Australia). The system is used to identify the sources of block instabilities (detachments) over several months to estimate the volumes of rock detached and their frequency over the period of observation.

The system consists of two units. Each unit includes a box containing a high-resolution digital single-lens reflex (DSLR) camera (Nikon D850) controlled by a Raspberry Pi microcomputer. The system allows the collection of synchronised images at different periods. The images are downloaded remotely and processed automatically on a server to obtain a 3D model (e.g. 3D point cloud and mesh). The system also includes a new in-house web interface that allows the automatic comparison of 3D models obtained at various periods (change detection) and, therefore, to track and measure rock volume detachments. The web interface also allows the user to validate the identified detachments by visual comparison of the section of the original images where the difference was detected.

A detailed analysis of the evolution of the rock surface, volumes and frequency of the rocks dislodging from the highwall over a period of several months is provided. This information constitutes valuable data for a detailed inventory of the rockfall spatial-temporal occurrence and magnitude. The data allows correlation of the occurrence of rockfall events with the rock lithology and weather conditions (e.g. rainfall events), confirming the capability of the system to generate useful data that would otherwise require extended periods of direct observation.

Keywords: *slope monitoring, rockfall, surface mining, photogrammetry*

1 Introduction

In open cut mining operations, where safety is paramount, detailed information on rock mass structural conditions and on the evolution in time of excavated slopes is crucial to ensure safe and continuous mining operations. Monitoring of slopes is, therefore, a pivotal activity within surface mine operations that allows the ensuring of safety for personnel and machinery, and reduces any costs associated with potential

interruptions due to unexpected instabilities. Two main requirements are generally recommended for slope monitoring in surface mining operations (Sharron & Eberhardt 2020): tactical monitoring focuses on the safety of operating crews and equipment at the bench and inter-ramp scales, and strategic monitoring addresses the stability of the inter-ramp and overall slope of the entire area.

Various slope monitoring methods are currently available to engineering practice, each of them showing different advantages and weaknesses (Read & Stacey 2010). Continuous developments now allow identification of the most suitable technique according to site-specific environmental conditions, accessibility and the dimensions of the monitored surface (e.g. object), expected accuracy and spatial/temporal resolution of the data, and available budgets (Scaioni et al. 2014). Giacomini et al. (2020) have recently proposed a novel autonomous terrestrial stereo-pair photogrammetric monitoring system to monitor sub-vertical rock surfaces located in surface mining environments. The system, specifically developed to face particularly rough site conditions (dust, operational activities, transport vibrations) allows detection of the volumes of rock detaching from the rock surface at specific epochs and over user-defined periods of observation. If required, the collected images can also be used for geostructural mapping but the system is designed for continuous monitoring.

The system includes two standalone units synchronised via the onsite-available wi-fi network: each unit consists of a camera box, a battery box, 60 watt solar panel and a steel post embedded into a grader tyre filled with concrete (Figure 1a). The camera box consists of a weather-resistant steel box containing a single-board microprocessor (Raspberry Pi 3 Model B, or RPi) and a full-frame DSLR camera (Figure 1b). The camera used with the prototype was a full-format Nikon D810 with a 50 mm fixed focal lens (AF-S Nikkor 50 mm f/1.8 G lens). The image sensor has a resolution of 36 megapixels and a very high extended sensitivity range. The latter ranges from ISO32 to ISO51200 and allows for low-light and night-time acquisitions (Bruno et al. 2021, 2022). The camera is connected to an RPi which allows control of the image acquisition via the open-source library gPhoto (www.gphoto.org). Images can be taken at any time with any specific settings using a predefined trigger table. The two units capture synchronised stereo-pair digital images that are then available to the user to conduct structural analyses and identify the rock detachments by means of 3D models.

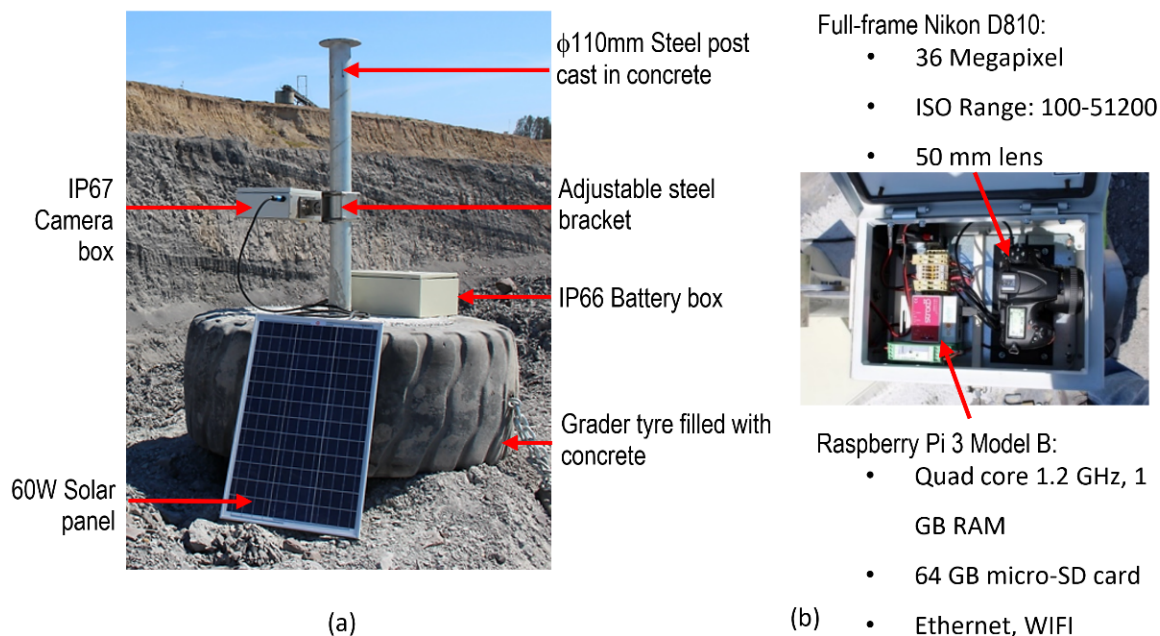


Figure 1 Prototype developed during a government-funded project: (a) Installed system; (b) Close-up of the camera box (Giacomini et al. 2020)

Initial trials have shown the system as a valuable and cost-effective alternative to more common expensive monitoring solutions, especially for areas with a high level of hazard where specific details are required over a short period of time (Giacomini et al. 2020). However, in its initial design, some limitations have also been

identified. The installation does not allow small position adjustment, or the use of different lenses or different camera bodies. Noise related to unexpected movements of the two units due to mining activity and image disturbances due to reflected light within the camera enclosure have also been observed. Finally, manual image processing is quite cumbersome and time-consuming.

Over the last two years, the system has been redesigned to better account for an easy installation in different locations and to permit a more flexible set up of the camera box (including different lenses). Additionally, a fully automatic processing pipeline for generating the 3D models (including change detection and monitoring) at user-defined frequencies via a graphical user interface was implemented. In this paper, details of the redesigned monitoring system will be presented as well as its application to a mine site located in the Hunter Valley, New South Wales.

2 Design of the new system

The redesign process investigated the efficiency and applicability of two designs named Design A and Design B (Figure 2). This first camera enclosure's design (Design A) focuses on maximum accessibility to the camera and lens, achieved through a fully removable cover (Figure 2a) made from folded stainless steel sheet metal bolted to a thin frame. The front of the cover contains an ND filter (transparent glass) for the camera lens. The base of the enclosure is made of a flat steel plate with a set of mounting rails to accommodate the camera. An O-ring groove is also machined around the perimeter of the baseplate. Design B has the same overall dimensions and appearance as Design A, however, the cover of the enclosure is secured to the base by two custom hooks at the front and an over-centre latch at the rear. The two hooks act as hinges and the over-centre latch applies downward pressure to the entire cover. The front face of the enclosure is attached permanently to the base and supported by a gusset on each side. While fixing the front face and containing the view port to the base of the enclosure is highly beneficial for alignment, it also introduces new challenges to seal the enclosures and soft rubber tape is therefore used for this purpose. In both designs a $5/8'' \times 11$ TPI screw was used to attach a reflective prism to survey the camera enclosure position (Figure 2c).

A set of mounting rails attached to the base of each enclosure is used to secure the correct positioning of the camera to the enclosure. Two potential camera bodies have been considered for the design: the Nikon D810 and the Nikon D850. The camera can be locked to the baseplate by a screw and two pins have been manufactured to secure its orientation on the baseplate (Figure 3). The system has also been designed for three different lenses: 50 mm, 85 mm and 105 mm fixed focal lens.

A new mounting bracket (Figure 4a) secures the camera enclosure to a steel post and facilitates manual adjustment in multiple directions according to the desired orientation (Figure 4b).

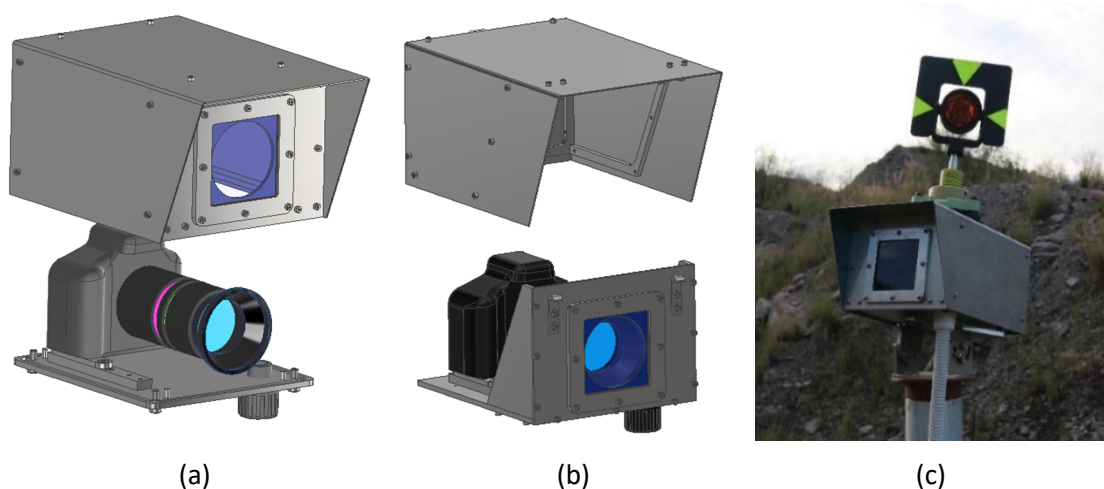


Figure 2 Camera enclosure: (a) Design A; (b) Design B; (c) Camera enclosure with a reflective prism

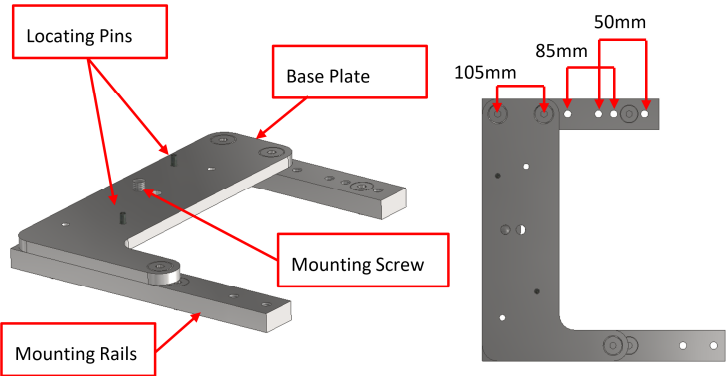


Figure 3 Details of mounting rails allowing for different cameras and lenses to be installed

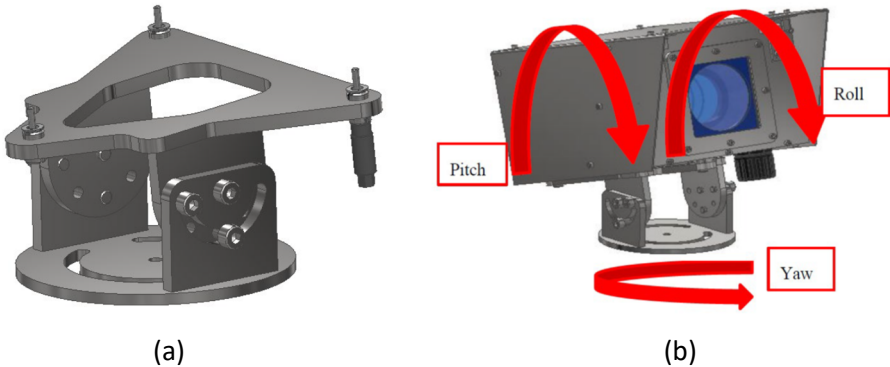


Figure 4 (a) Mounting bracket for camera enclosure; (b) Rotation directions allowed

The mounting bracket can be attached to a steel post embedded into a grader tyre filled with concrete. Similarly to its initial design, the steel post is 1.5 m-high and its diameter is 100 mm. It includes a 150 mm plate with two mounting holes where the mounting bracket can be attached. Figure 5 shows the whole system installed in the field. While the concrete-filled grader tyre ensures the stability of the system by minimising its movement it is not very practical to move around, and it is mainly recommended for long-term monitoring. More flexible foundations are currently under consideration and trials.



Figure 5 Picture of the whole redesigned system as installed at the mine site

The heart of the photogrammetry system is the electronic hardware and software that control the cameras. The cameras take images while the microcomputer and power electronics allow the system to function autonomously. A similar design of the electronics has been considered for the new system (Figure 1b). The main difference with the initial design resides in the separation of the electronics from the camera enclosures. The new electrical enclosures (Figure 6) have sufficient room for all existing components to be accommodated. The set up also provides easy access to USB and local area network (LAN) ports of the RPi for installation. Cable glands originally used in the previous enclosures have also been replaced with a 20 mm conduit which is sufficiently large for the extension USB cables and power cords and has ample room for the addition of new cables for sensors or potential new configurations.

Each camera unit is controlled by a small single-board computer, namely a RPi. The RPi is connected via USB to the DSLR camera, allowing for communication and control. Power requirements for the system consist of 12 V DC and 6 A (drawn during image capture only). The unit is also equipped with an uninterruptible power supply (UPS) that allows safe shutdown should the power be suddenly lost. The RPi compact single-board computer has all the basic functions of a full-sized desktop computer. The model being used is the RPi Rev 1.2 with the Raspbian Bullseye operating system installed and running Debian version 11. The RPi allows the writing and uploading of scripts to the device in various languages: this action can then be executed directly or scheduled to run autonomously. Most scripts have been written in Python 3.9 and some in Bash, allowing the incorporation of new functionalities. While the system is designed to be autonomous, the initial setup of the system requires using a laptop to communicate with both camera units to calibrate site-specific details.

The power can be provided from custom-built solar panels and batteries (Figure 1) or a communication sled/trailer provided by the mine site. Assuming a 15-minute capture interval with the images scheduled to upload every 10 minutes, a battery voltage of 12 V and a discharge period of three days, the minimum battery capacity is about 30 Ah. Therefore, two 12 V 24 Ah batteries in parallel (20-hour rate deep cycle batteries in parallel give a total capacity of 48 Ah) are sufficient to power one system for three days. However, a bigger capacity might be required if images are captured at smaller time intervals or if the sun should not be available for more than 36 hours.

As an example, the mine site where the new system was initially trialled provided a communication sled to power the system. The communication sled consisted of two solar panels, a box containing an array of lead-acid batteries, and another box containing electrical components such as switches, transformers and circuit breakers. The communications sled had an output voltage of 24 V DC, however, the monitoring equipment requires 12 V DC. As such, a DC-DC voltage converter was also installed, which provided the appropriate voltage for the monitoring equipment. In absence of wi-fi connection available on site, a Telstra 4G dongle was attached to both RPis (Figure 6), allowing the project team direct remote access to the system and uploading of the images into the server for processing.

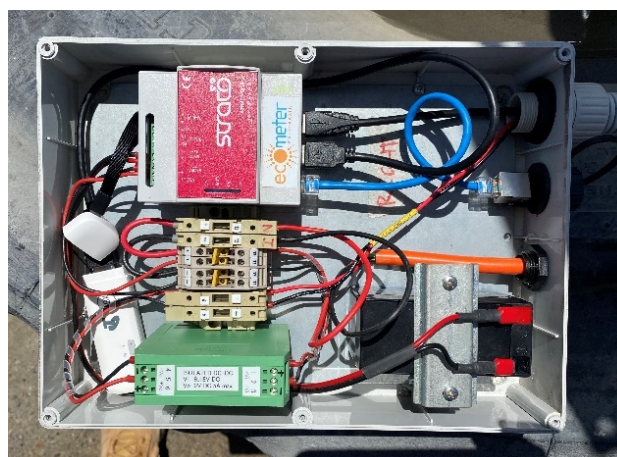


Figure 6 Electronic enclosures which include Raspberry Pi 3 Model B, uninterruptible power supply (UPS) battery, terminal blocks, power supply and a Telstra 4G dongle for internet access

3 Camera sensors

The camera's characteristics are crucial to assess results obtained using stereo-photogrammetry. Since both cameras, the Nikon D810 and D850, are full-frame cameras with the same sensor size, the effect on the field of view, if equipped with the same optics, is the same (35.9 × 24 mm). Pixel densities will vary as the cameras have different megapixel counts. Tables 1 and 2 summarise the key properties of the two cameras and four lenses used in the application, respectively.

Table 1 Camera properties

Camera	Nikon D810	Nikon D850
Release year	2014	2017
Width of the camera sensor (mm)	35.9	35.9
Height of the camera sensor (mm)	23.9	23.9
Width of image (pixel)	7,360	8,256
Height of image (pixel)	4,912	5,504
Sensor pixel size (µm/pixel)	4.88	4.35

Table 2 Lens properties

Lens	AF-S NIKKOR 35 mm f/1.8 G	AF-S NIKKOR 50 mm f/1.8 G	AF-S NIKKOR 85 mm f/1.8 G	AF-S NIKKOR 105 mm f/2.8 G
Focal length (mm)	35	50	85	105
Angle of view on FX (diagonal) (deg)	63	47	30	23.3
Calculated field of view angle on FX (horizontal) (deg)	54.3	39.5	23.8	19.4
Calculated field of view angle on FX (vertical) (deg)	37.7	26.9	16.1	13.0
Length (distance from camera lens mount flange) (mm)	71.5	52.5	73.0	126.4

Based on the specification of the camera and the lens, it is possible to calculate the image footprint and the ground sample distance (GSD) based on the distance from the object. When the subject is perpendicular to the object of interest, the horizontal and vertical image footprint of a specific lens can be calculated as:

$$\text{Subject size} = 2 \cdot \tan\left(\frac{FOV}{2}\right) \cdot d \quad (1)$$

where subject size is the vertical or horizontal footprint, FOV is the field of view of the lens and d is the object distance. The object distance is the normal distance between the camera and the object to be captured.

The GSD corresponds to the corresponding size of one pixel on the object, i.e. it defines the distance between two consecutive pixel centres measured on the ground (Thoeni et al. 2018). The bigger this value, the lower the resolution. This is not affected by differences in the field of view in the horizontal and vertical directions, only by the dimensions of the sensor, resolution and focal lens used. The GSD (in mm) can be calculated as:

$$GSD = \frac{d \cdot p}{f} \quad (2)$$

where d is the object distance (m), p is the size of the pixel on the sensor (µm/pixel) and f is the focal length (mm).

4 Development of image processing interface (Slope Monitor)

A fully automatic processing pipeline to generate 3D models of the rock surface (including change detection and monitoring) at user-defined frequencies was implemented. The processing is achieved via three components: a processing server, a database (PostgreSQL) and a user web interface (Figure 7). The data exchange between the processing server and the monitoring system is currently happening via Google Drive, i.e. the images are automatically synchronised via Google Drive. An alternative option is the use of a site-specific file transfer protocol (FTP) server. The processing pipeline was developed by the University of Parma in Italy and is referred to as *Slope Monitor*.

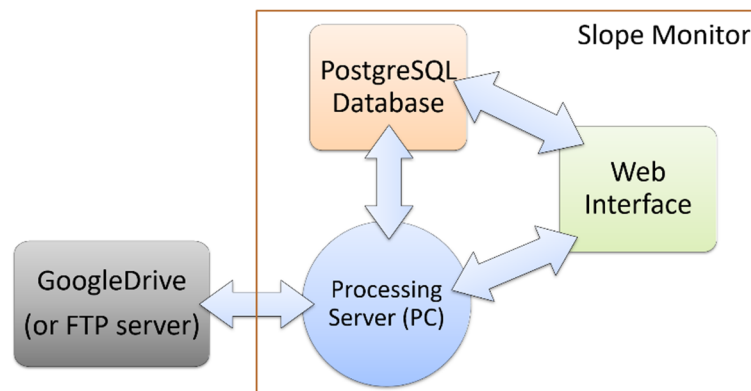


Figure 7 Processing system architecture

The web interface provides the user with the ability to manage the automatic processing pipeline. This includes specifying how the images are processed and what type of results the user plans to obtain, such as 3D point clouds, 3D textured triangulated mesh (useful for geotechnical mapping), a digital elevation model as 2.5D raster image, differences between 3D models and/or 2.5D raster images (change detection), and the identification of detachments and movements in the rock mass.

The web interface automatically accesses the processing server. The processing server currently uses Agisoft Metashape (Agisoft 2023) to build the 3D model. Nevertheless, the interface is generic and it also allows the use of other photogrammetry packages. The Metashape-generated 3D models are then stored in a PostgreSQL database. The processing server then accesses the data for further processing. This includes alignment of models through iterative closest point techniques (Besl et al. 1992), generation of 2.5D raster images, change detections and identification of detachments. Figure 8 shows an example of detachment (a rockfall event) details. General information about the date and time of the event, block position, its dimensions and volume, and any comments, are reported on the top left. On the bottom left, the reference image can be compared to the image after the detachment (the contour of the detached block is represented in red in both images). The location of the block in the wall is highlighted with a red rectangle in the top right of the image while a 3D model of the block is shown at the bottom right of the image. All relevant algorithms are specifically developed by the research team.

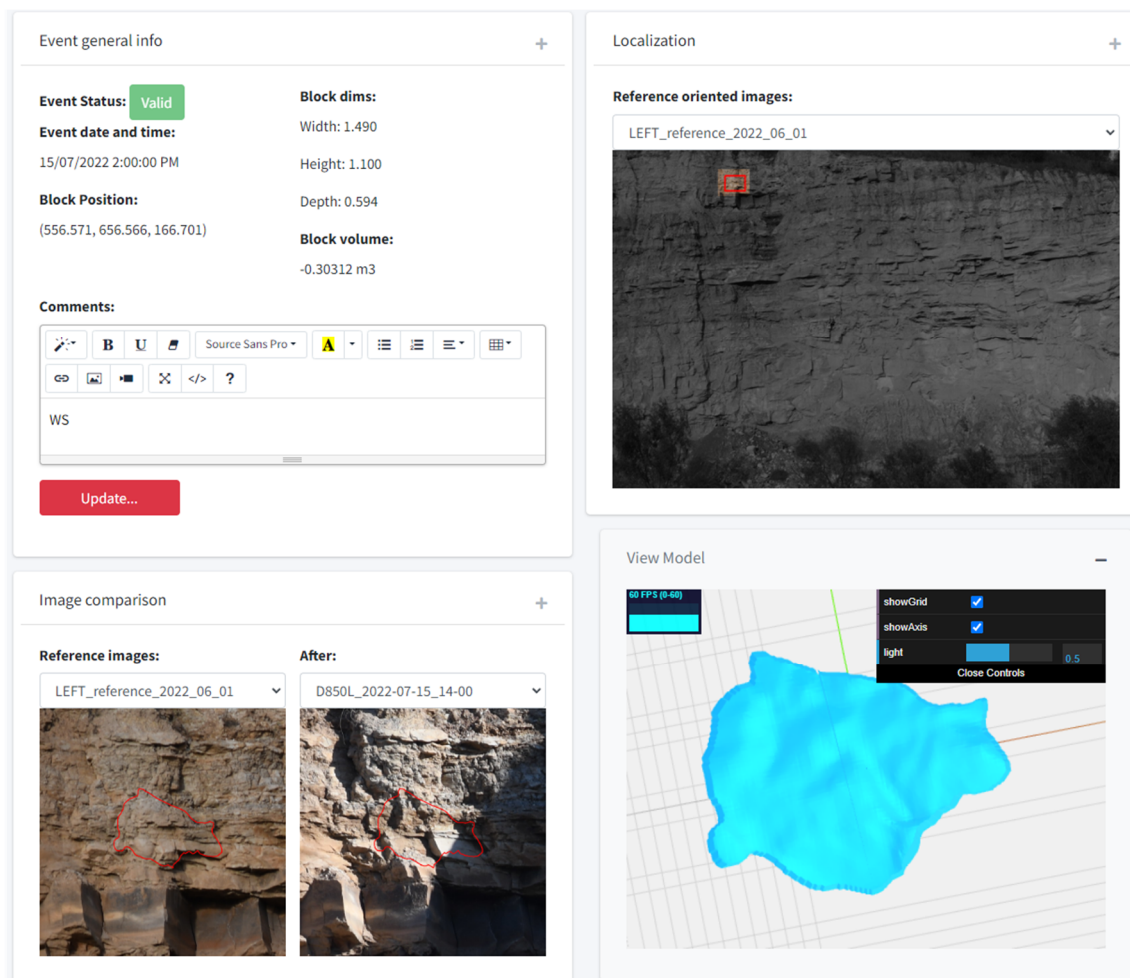


Figure 8 Example of a rockfall event's details

5 Application and results

5.1 Site description and system installation

In May 2022 the system was installed at a mine site in the Hunter Valley, where access was provided to an old weathered highwall so that the work of this project would not interfere with mining operations. An initial five-month monitoring phase was used to trial and improve the system set up, solve some initial issues encountered with the power supply and unreliable hardware components, and gather and calibrate the most appropriate processing parameters. Monitoring of the rock face started on 11 November 2022 and is ongoing. The highwall is about 29 m high and 35.6 m wide, with a stratigraphy including an upper layer of weathered fine sandstone followed by a layer of weathered coal, interbedded mudstone and fine sandstone, and a thick layer of sandstone (overlying a weathered coal seam covered by the bench).

The two camera units have been positioned at about 87 m from the wall. Enclosures A (Figure 2a) and B (Figure 2b) were used for the right and left cameras, respectively. The cameras have a base length of 32.6 m and are orientated in a slight convergent pose to ensure maximum overlap. The GSD is 7.6 cm. Figure 9 shows the left and right images of the section of highwall captured by the left and right cameras, respectively. A reflector prism was also set up on each camera unit to measure its precise position (Figure 2c) using a total station (Leica MS60). A total of 32 ground control points (GCPs) on the highwall were surveyed (Figure 10) using the same total station. The GCPs were used to estimate the exterior orientation parameter of the cameras, which have been preliminary calibrated in an ad hoc calibration field at the University of Newcastle. They also provide check data for possible camera movements during the monitoring period.



Figure 9 Example of (a) left and (b) right captured by the monitoring system

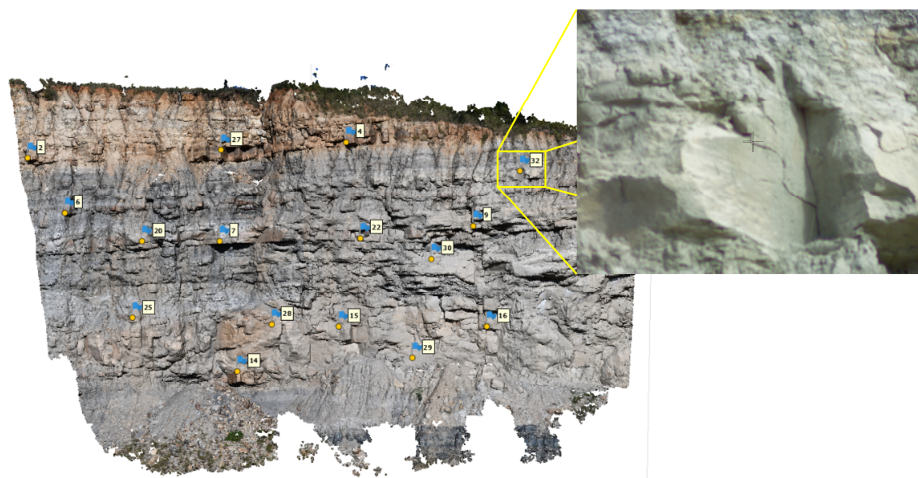


Figure 10 Natural features used as GCPs. The zoomed image is an example of an image taken with the total station (Leica MS60) of point 32 (the crosshair indicates the measured location of the GCP)

5.2 Multi-temporal data analysis

Stereo-pairs of images were acquired every two hours by the two units. However, due to the low rockfall activity of the wall, only images acquired at 8 am every day were analysed to evaluate the effectiveness of the system for change detection and volume estimation in the context of the temporal and spatial occurrence of rockfall events. The data were grouped to correspond to 15 periods of monitoring from June 2022 to April 2023. Table 3 shows the relevant dates and number of days for each of the nine monitoring periods. Maximum and total rainfall data are also reported.

5.3 Change detection analysis

Slope Monitor was used to process the data and obtain the rockfall events data for each period. Figure 11 shows an example of the 2.5D raster difference obtained for monitoring period A1. The red colour represents negative differences while blue indicates positive differences. A negative difference usually corresponds to actual block detachments while a positive difference can represent movement or accumulation of material (debris). Intuitively, not all the differences are actual detachments or rock movements. Without filtering, the process identifies all differences including real events (i.e. true rockfall detachments) and false positives (i.e. shadow, vegetation, moving objects such as animals or machines). Figure 12 shows examples of false positives. To reduce the number of false positives, the current change detection algorithm in Slope Monitor focuses on negative differences only, i.e. block detachments. However, this limitation could potentially induce the neglect of positive movements which could, in turn, be used as an early warning of block detachment. Additional work is therefore required to develop a more robust algorithm that can accurately differentiate detachments from movements and automatically remove false positives.

Table 3 Information related to the monitoring periods

Period	Date reference	Date comparison	Days within period	Maximum rainfall during period (mm)	Total rainfall during period (mm)
A1	1/06/2022	15/07/2022	44	97	229.4
A2	15/07/2022	29/07/2022	14	3	4.8
A3	29/07/2022	19/08/2022	21	26.2	50.6
A4	19/08/2022	16/09/2022	28	19	20.4
A5	16/09/2022	5/11/2022	50	30.2	181
A6	5/11/2022	15/11/2022	10	39	59
A7	15/11/2022	1/12/2022	16	1.2	1.2
A8	1/12/2022	1/01/2023	31	4.4	11.6
A9	1/01/2023	8/01/2023	7	12.6	18
A10	8/01/2023	26/01/2023	18	5	18.4
A11	26/01/2023	14/02/2023	19	21.2	41.8
A12	14/02/2023	25/02/2023	11	41.6	77.8
A13	25/02/2023	27/03/2023	2	28.8	60.8
A14	27/03/2023	31/03/2023	32	35	50.6
A15	31/03/2023	24/04/2023	24	8	20.6

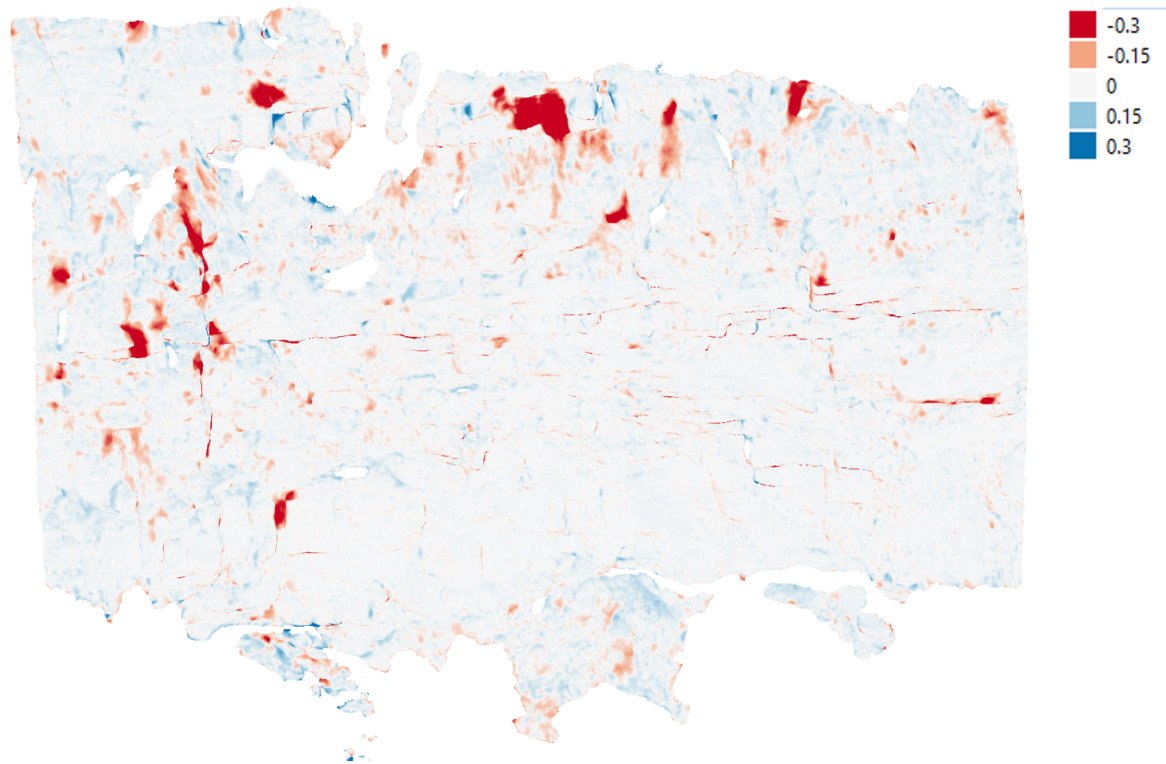


Figure 11 2.5D raster difference of the monitoring period A1

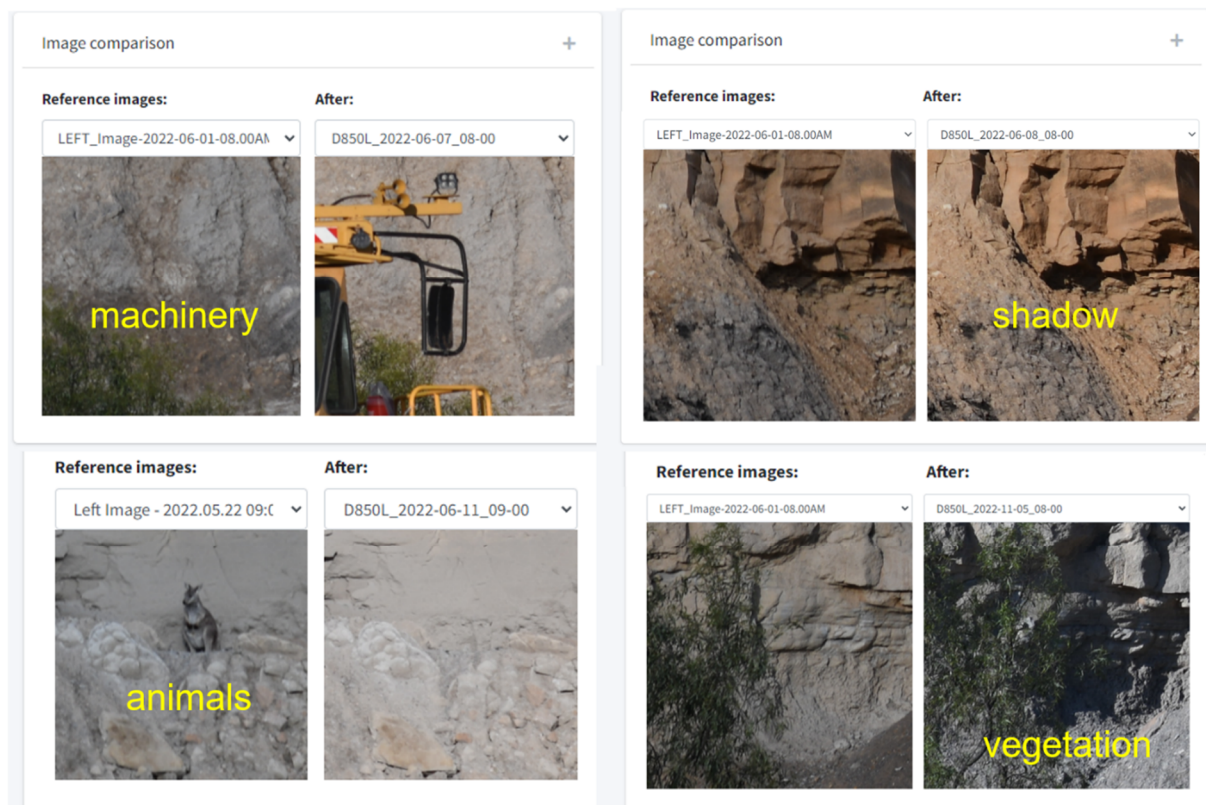


Figure 12 Examples of false positives. Comparison between the reference image and the image used for the change detection

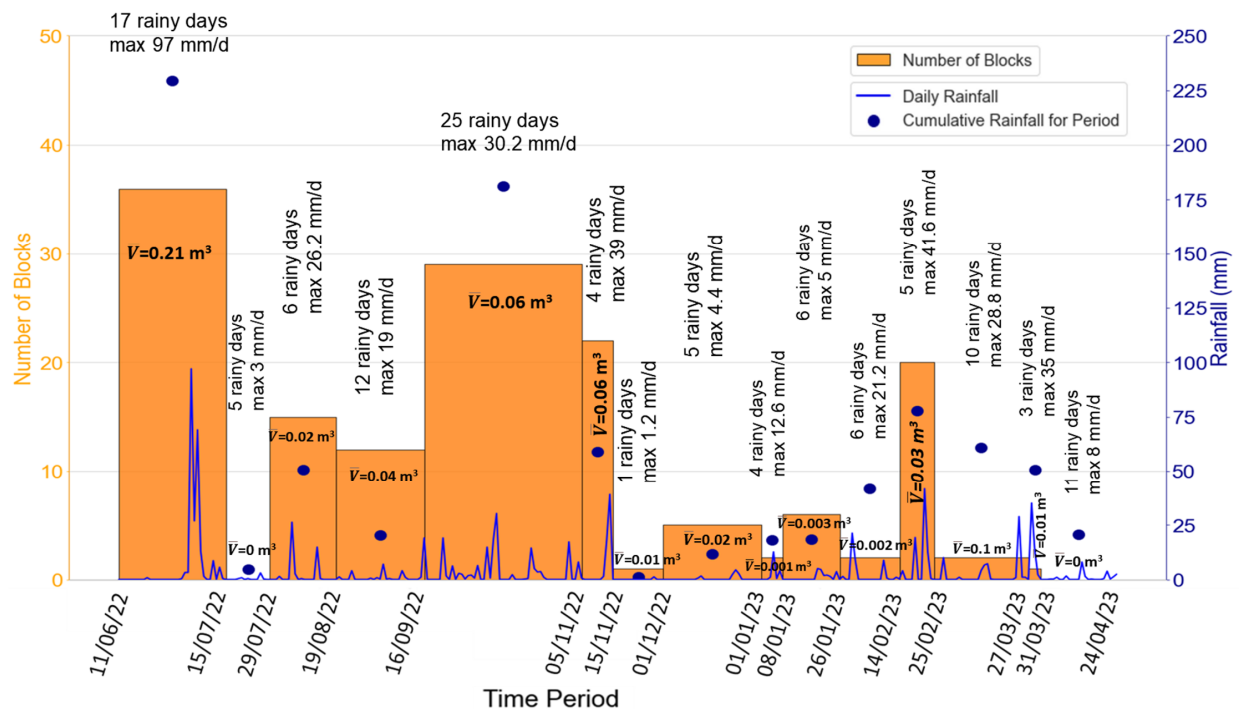
5.4 Results

This section summarises the main results of the monitoring campaign carried out between June 2022 and April 2023 at the trial application site. Table 4 lists the number of events per monitoring period, the frequency of events per week, and the minimum and maximum estimated volume for each period. Similar data is shown in Figure 13, where the rainfall data is also plotted with the number of events per period (and the estimated average volume of rock during each period). The results allow us to investigate the correlation between rockfall events and rainfall while providing an accurate estimation of the rockfall frequency, which is crucial for a comprehensive risk assessment. For example, period A1 evidenced the highest rainfall event with 97 mm per day and also the largest number of events. Periods A2 and A15 did not record rockfall events and show some of the lowest values of rainfall (mm/d) of the overall monitoring period.

Figure 14 presents an overview of all blocks detected by the multi-temporal data analysis and infers the location of the blocks detached during a particular monitoring period. It also allows the identification of critical areas of detachments or material layers particularly affected by detachments. For example, it can be observed that the left-hand side of the highwall section is more susceptible to rockfalls. Figure 15 summarises the results in terms of volume per material layer. The data indicates that most of the rockfall activity comes from the mudstone/sandstone layer. However, the biggest blocks detached were from the weathered sandstone layer.

Table 4 Summary of recorded rockfall events

Period	Number of events	Frequency in events per week	Min volume (m ³)	Max volume (m ³)
A1 (44 days)	38	6.0	0.006	1.521
A2 (14 days)	0	0.0	0.000	0.000
A3 (21 days)	15	5.0	0.003	0.090
A4 (28 days)	12	3.0	0.001	0.109
A5 (50 days)	29	4.1	0.003	0.624
A6 (10 days)	22	15.4	0.004	0.351
A7 (16 days)	1	0.4	0.012	0.012
A8 (31 days)	5	1.1	0.003	0.061
A9 (7 days)	2	2	0.001	0.002
A10 (18 days)	6	2.3	0.001	0.008
A11 (19 days)	2	0.7	0.001	0.004
A12 (11 days)	20	12.7	0.002	0.141
A13 (2 days)	2	7	0.001	0.201
A14 (32 days)	1	0.2	0.007	0.007
A15 (24 days)	0	0.0	0.000	0.000


Figure 13 Summary of the number of blocks identified in each monitoring period, their total volume and rainfall data for the relevant period

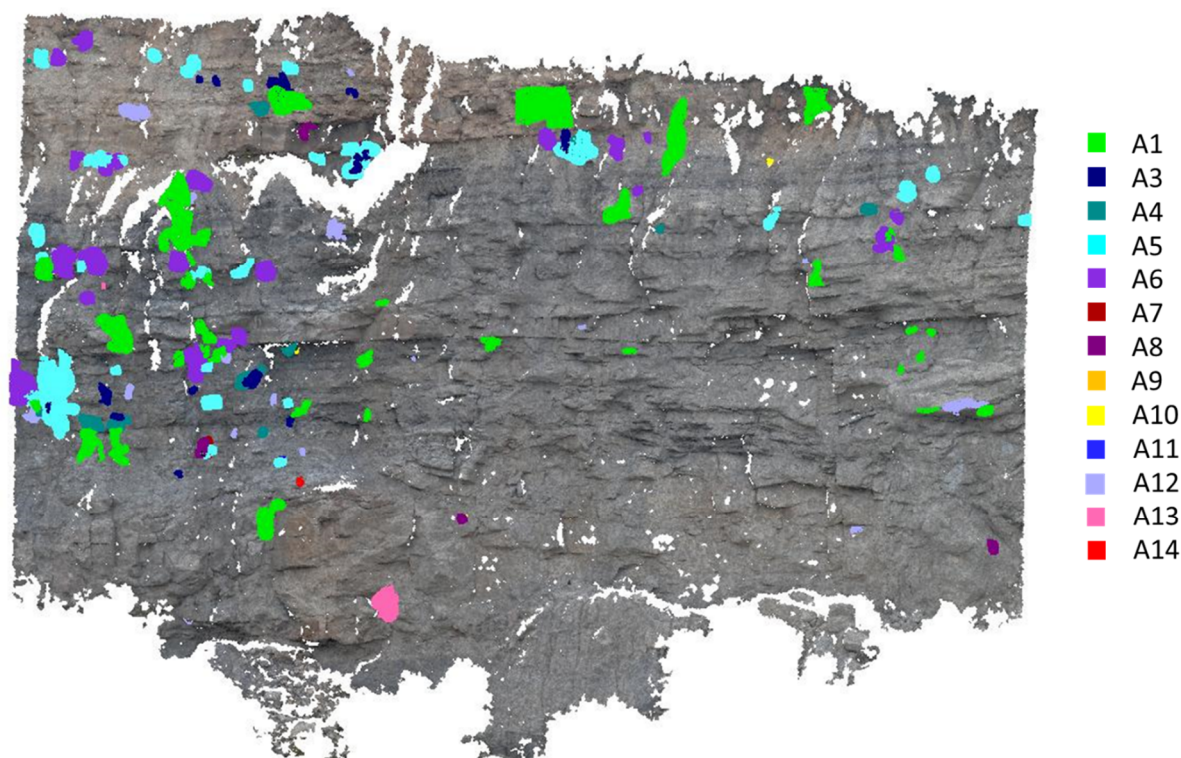


Figure 14 Identified blocks colour-coded by the period in which they occurred. Note that no blocks were identified during periods A2 and A15

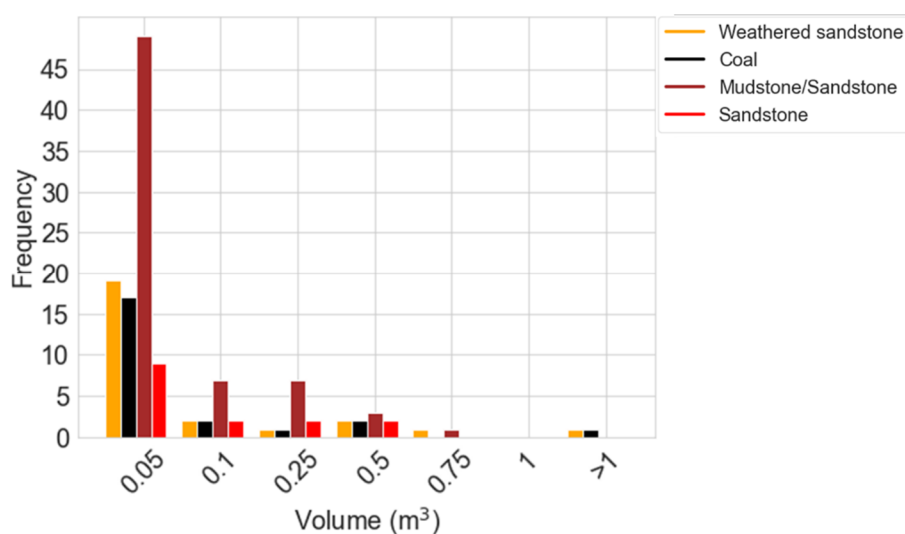


Figure 15 Volume-frequency (total number of events during the monitoring period) relation of rockfall events per material recorded over all monitoring periods

6 Conclusion

In this paper, the redesign of a fixed-base stereo-photogrammetry monitoring system specifically devoted to surface mining applications was presented. The implementation of an automatic processing pipeline and the development of a user-friendly interface contribute to the enhancement of the system. The new system is based on learnings acquired from the development and application of a first system prototype designed by the authors.

One main aspect of the new design is the separation of the camera from the rest of the electronic hardware, resulting in a significant increase in flexibility. The new camera enclosure can also accommodate different cameras and lenses, broadening the system's applicability to locations where diverse distance/positioning from the object (rock face) is required. A completely new mounting bracket has also been designed to allow an easy fine adjustment of the orientation of the camera. These improvements were crucial to increasing flexibility and facilitate easy and quick installation. Design B was identified as more practical, so it is therefore preferred for future applications.

A fully automatic processing pipeline for generating 3D models (including change detection and monitoring) at user-defined frequencies was implemented. The processing is achieved via three components: a processing server, a database and a user-friendly graphical web interface. The data exchange between the processing server and the monitoring system is currently via Google Drive; i.e. the images are automatically synchronised via Google Drive. Alternatively, the system can rely on a site-specific FTP server. The processing pipeline was developed by the University of Parma and is referred to as Slope Monitor. A user-friendly web interface was designed to provide the user with the ability to manage the automatic processing pipeline and set parameters for the change detection analysis.

The monitoring system was installed at a mine site in the Hunter Valley in May 2022. Access was provided to an old weathered highwall so that the work of this project would not interfere with mining operations. The monitoring period lasted around 11 months. It was subdivided into 15 periods based on rainfall events since a correlation between rainfall and rockfall events was expected. The analysis allowed identification of the number of rockfall events per period, their approximate volume and shape (not included here due to space limits). It was also possible to identify from which material layer the blocks detached. The data collected allow mine operators to assess the possible correlation between rockfall events and rainfall for future predictions while providing an accurate estimation of the rockfall frequency, which is crucial for a comprehensive risk assessment.

Acknowledgement

This study was financially supported by the Australian Coal Association Research Program (ACARP). The authors are extremely grateful for the support from industry monitors Brittany McArdle, Gareth Johnson, Dan Stolberg and John Latilla, and for their helpful comments and suggestions. The authors also thank Patrick Tyrrell for his support and assistance as project coordinator.

The authors also wish to acknowledge the contributions of Jake Vaha, Eric Turvey and Mathew West. Jake assisted with the redesign of the system, Eric conducted the data analysis for the calibration and Mathew assisted with the fieldwork. The support of the University of Newcastle facilities is also gratefully acknowledged.

References

- Agisoft 2023, Agisoft Metashape, *computer software*, www.agisoft.com/downloads/installer
- Besl, PJ & McKay, ND 1992, 'Method for registration of 3-D shapes', *Sensor Fusion IV: Control Paradigms and Data Structures*, vol. 1611, pp. 586–606.
- Bruno, N, Forlani, G, Giacomini, A, Roncella, R, Thoeni, K 2021, 'Influence of illumination changes on image-based 3D surface reconstruction', *ISPRS - International Archives of the Photogrammetry, Remote Sensing and Spatial Information Sciences*, XLIII-B2-2021, pp. 701–708.
- Bruno, N, Roncella, R, Diotri, F, Thoeni, K, Giacomini, A 2022, 'Photogrammetric digital surface model reconstruction in extreme low-light environment', *Remote Sensing*, vol. 14, no. 15.
- Giacomini, A, Thoeni, K, Santise, M, Diotri, F, Booth, S, Fityus, S & Roncella, R 2020, 'Temporal-spatial frequency rockfall data from open-pit highwalls using a low-cost monitoring system', *Remote Sensing*, vol. 12, no. 15.
- Read, J & Stacey, P 2010, *Guidelines for Open Pit Slope Design*, CRC Press, Boca Raton.
- Scaioni, M, Longoni, L, Melillo, V & Papini, M 2014, 'Remote sensing for landslide investigations: an overview of recent achievements and perspectives', *Remote Sensing*, vol. 6, pp. 9600–9652.
- Sharron, R & Eberhardt, E 2020, *Guidelines for Slope Performance Monitoring*, CSIRO Publishing, Melbourne.
- Thoeni, K, Santise, M, Guccione, DE, Fityus, S, Roncella, R & Giacomini, A 2018, 'Use of low-cost terrestrial and aerial imaging sensors for geotechnical applications', *Australian Geomechanics Journal*, vol. 53, no. 3, pp. 101–122.